Fermilab Library
0 1160 0041828 9

— FPRINT-95-20
36

Nuclear Force and its Long Range Component of the van der Waals Type

Tetsuo Sawada

Institute of Physics
University of Tsukuba
Ibaraki , 305 ,Japan

FERMILAB
MAY 1
LIBRA

Abstract

In search for the possible long range force between hadrons, S-wave phase shift data of the proton-proton scattering are analysed. In the analysis, the once subtracted Kantor amplitude is calculated, and the one-pion exchange contribution is separated. The remainder of the Kantor amplitude has a huge cusp at the threshold with the attractive sign. It is shown that such a cusp cannot be fitted by the spectral function of the two-pion exchange, since it starts at $t = 4\mu_\pi^2$. The cusp is fitted by a potential of the long range type with the asymptotic form of $V(r) \sim -C/r^\alpha$. After the chi square search, it turns out α is $6.1 \sim 7$ and C is positive and has the strength of the strong interaction. It is consistent with the potential of the strong van der Waals force. The transition from the London type to the Casimir-Polder type of the van der Waals interaction is examined. Possible experiments to observe directly such a long range force in the nuclear force are also indicated .

1. Introduction

Sixty years ago, Yukawa[1] proposed to understand the nuclear force in terms of the "heavy quanta", which satisfied the Klein-Gordon equation with mass, and at that time the only particle which mediated the force was the light quanta, the photon. The experimental dicovery of the pion was regarded as a triumph of his idea, and people believed that the nuclear potential $V(r)$ would be constructed from the meson theory, namely from the N-π vertex and also from the four-pion vertex, in short time. The calculations of the two-pion exchange potential by purterbation turned out to be too small compared to what was required in experiments, and the original programms turned out too ambitious. Efforts in such a direction are still going on in a little retreated form. In the recent works[2], which seem to be closest to the original programm, the amplitudes of the pion-nucleon and the pion-pion are used as inputs to caluculate the spectral function $A_t(s,t)$. And in the calculation, the analytic continuation and the use of the generalized unitarity relation are necessary. There are another type of successful approaches[3, 4, 5], which are something between the dispersion approach and the original one-boson exchange model. The most important difference is that Δ is treated as an independent particle, and therefore the Δ-N-π vertex is added to the original vertices.

Although there are a variaty of approaches to the nuclear potential from the meson theory, people have shared a view in common that in the outermost region of the potential, the one-pion exchange (OPE) term dominates. Therefore we can expect to observe the 'pure' OPE contribution in the very low energy phenomena of the P-wave. In terms of the language of the r-space, this is because the centrifugal force prevents for the very low energy particle to approach to the inner domain and the particle picks up only the information of the one-pion exchange potential in the process of the scattering. If we restate the same process in terms of the spectral function $A_t(s,t')$, the partial wave amplitudes $h_\ell(\nu)$ are the projections with factors $Q_\ell(1 + t'/2\nu)/2\nu$, which damp as $O((4\nu/t')^{(\ell+1)})$, therefore the spectral function are suppressed in $t' > 4\nu$ and the suppressions are more effective

for higher ℓ. Since the phase shift data of the very low energy are available only for S snd P waves, people expected that the P-wave phase shift traces the one-pion exchange (OPE) curve when the incident energy T_{lab} decreases to zero. People were surprised when the Wisconsin data[8] did not show such behavior (see fig.4 in Section 4). Instead, the P-wave phase shift behaves as if there were no pion pole. Reactions of physicists at that time range from an optimistic one, that when we fully understand the two-pion exchange potential the difficulty will be solved simultaneously, to a pesimistic one that the pion does not exist. However I believe it is possible to adopt a third point of view[11] that there exists a long range force of attractive sign which cancells the repulsive OPE potential. Notwithstanding the beautifulness of Yukawa's idea and subsequent discovery of the pion, there is no apriori reason that the nuclear force is strictly short range. This is so, especially when the nucleon is composite and the basic force between the constituent particles is the Coulombic type. In such a case, it is not surprising that the dispersive force of the long range nature appears as the secondary force. Therefore it must be a good idea to ask to Nature what the real world is.

In this paper we shall consider the fundamental problem whether the hadron-hadron interaction involves the long range force. Because of the high precision, the low energy p-p data provides an ideal place to search for the possible long range potential. In terms of the spectral function $A_t(s,t')$, we are going to determine the functinal form for small t', especially in $t' < 4\mu_\pi^2$ where in the meson theory $A_t(s,t')$ is strictly zero, except for the δ-functin of the one-pion exchange. Although it is desirable to analyse the P- or higher partial waves[12], almost all of the precise data of the very low energy region are available only in the S-wave. Therefore, instead, we shall analyse the once subtracted S-wave amplitude $(h_0(\nu) - h_0(0))/\nu$, and whose projection function is $\{Q_0(1+2\nu/t')/2\nu - 1/t'\}$ which damps as $O((4\nu/t')^2)$, namely the suppression is the same as that of the P-wave. The very high precision[13] of the scattering length of ${}^1S_0$ of the p-p scattering, which is 0.06 %, permits us to introduce the once subtracted S-wave amplitude. Since the accuracy of the effective range is still high, namely 0.6 %, we can even use the twice subtracted

S-wave amplitude, and the effect of suppression for large t' of $A_t(s,t')$ is the same as that of the D-wave.

There are two prominent features in the low energy p-p scattering. The first one is the interference minimum[14] at $T_{lab} = 0.38248 \pm 0.00010 Mev.$, and which is useful in making the high precision determination of the coefficients of the effective range expansion. The second one is the appearace of the pole of the "anti-bound state" in the S-wave amplitude whose location is very close to the threshold. Such a pole causes the rapid change of the phase shift in the very low energy region and requires a special technique when we calculate the pricipal value integration of the imaginary part of the S-wave amplitude without losing the precision of the original data. Contrary to the pole of the ordinary bound state on the complex ν-plane, poles of the "anti-bound states" appear on the second Riemann sheet of ν. In terms of T_{lab}, which is proportinal to ν, the location of the pole is $T_{lab} = -1.031 Mev.$ on the second sheet, and therefore it dominates the rapid change of the phase shift of the S-wave of the p-p scattering in the very low energy region.

In the present article, we shall analyse the S-wave amplitude $h_0(\nu)$ in search for the possible long range force. The first thing to do is to select a quantity which is analytic in the neighborhood of $\nu = 0$ when all the forces are short range. The best-known such quantity is $\sqrt{\nu}\cot\delta_0(\nu)$ which accepts the effective range expansion of ν. However there is another such quantity, the Kantor amplitude[15] $K_0(\nu)$, which is defined by subtracting the contribution of the right hand cut from the amplitude $h_0(\nu)$. The Kantor amplitude is more suitable for our aim to observe the possible singularity at $\nu = 0$ arising from the long range force and to determine the strength C' and the power γ of the spectral function $A_t(s,t')$ at $t' = 0$. Moreover γ relates to the power of the asymptotic form of the long range potential by $V(r) \sim -C/r^{2\gamma+3}$. Another merit to use the Kantor amplitude is that we can eliminate the nearest singularity arising from the *short range* forces, the one-pion excange force in our case, and we can prepare the wider domain of analyticity, which enables us to observe the singularity of the long range force at $\nu = 0$ more easily when it actually exists.

In Section 2, we shall introduce the Kantor amplitude and rewrite it to the form of the contour integration. In Section 3, the Kantor amplitude is generalized to include the Coulombic distortion, in order to apply to the proton-proton scattering. In Section 4, the Kantor amplitude of the S-wave of the p-p scattering is calculated from the phase shift data of the energy dependent analysis. The once subtracted Kantor amplitudes $(K_0(\nu)-K_0(0))/\nu$ minus the one-pion exchange contribution are tabulated, which indicate a sharp cusp at $\nu = 0$. In Section 5, the relation between the potential and the spectral function is explained. As a preliminary study, the Kantor amplitude is fitted by one or two poles of the one-boson exchange type. In Section 6, the once subtracted Kantor amplitude of the S-wave is analysed, the chi square minimum is searched to determine the threshold behavior of $A_t(4m^2, t')$ at $t' = 0$. The results of the fits indicate the strong van der Waals interaction between protons. In Section 7, in order to confirm the van der Waals interaction, the transition from the London type to the Casimir-Polder type is examined. Possible new experiments to observe the strong van der Waals interactoin directly, is suggested. Section 8 is reserved for comments and discussions. One of the topics discussed is the reason why the long range force in the nuclear force has escaped our observation for such a long time when the strength of such a force is not a small correction to the short range interactions.

2. The Kantor Amplitude

In this section, we shall consider scatterings by a short range potential, and inclusion of the Coulombic potential will be done in the next section. It is well-known that

$$X_\ell(\nu) = \nu^{\ell+1/2} \cot \delta_\ell(\nu) \tag{1}$$

is regular at $\nu = 0$, and can be expanded in terms of ν, where ν is the momentum in the center of mass system squared. Partial wave amplitudes relate to the phase shifts $\delta_\ell(\nu)$ in the elastic region by

$$h_\ell(\nu) = \frac{\sqrt{m^2+\nu}}{\sqrt{\nu}} e^{i\delta_\ell(\nu)} \sin \delta_\ell(\nu). \tag{2}$$

From Eqs.(1) and (2),

$$\frac{h_\ell(\nu)}{\nu^\ell} = \frac{\sqrt{m^2+\nu}}{X_\ell(\nu) - i\sqrt{\nu}\,\nu^\ell} \tag{3}$$

Since we analyse the S-wave amplitude in this article, we set $\ell = 0$ hereafter, however equations for the higher partial waves are recovered if $h_0(\nu)$ is replaced by $h_\ell(\nu)/\nu^\ell$. The integral representation of the partial wave amplitude is

$$h_0(\nu) = \frac{1}{\pi}\int_{-\infty}^{-a/4} \frac{Im\, h_0(\nu')}{(\nu'-\nu)} d\nu' + \frac{1}{\pi}\int_0^\infty \frac{Im\, h_0(\nu')}{(\nu'-\nu)} d\nu' \tag{4}$$

where $\sqrt{a}$ is the smallest mass of the exchanged states. The right hand cut ($\nu > 0$) is the unitarity cut and whose spectral function $Imh_0(\nu')$ is determined directly from the phase shift data. By collecting the terms, which are calculated from the experimental data, in the integral representation of Eq.(4), the Kantor amplitude $K_0(\nu)$ is introduced by

$$K_0(\nu) = h_0(\nu) - \frac{1}{\pi}\int_0^\infty \frac{Im\, h_0(\nu')}{(\nu'-\nu)} d\nu' \tag{5}$$

, and Eq.(4) becomes

$$K_0(\nu) = \frac{1}{\pi}\int_{-\infty}^{-a/4} \frac{Im\, h_0(\nu')}{(\nu'-\nu)} d\nu' \,. \tag{6}$$

Equation(6) indicates $K_0(\nu)$ is regular at $\nu = 0$, and the nearest singularity occurs at $\nu = -a/4$. For p-p scattering, $a = \mu_0^2$, where μ_0 is the mass of the neutral pion. When we need the wider domain of analyticity, we subtract the contribution of the one-pion exchange, then a moves to $4\mu_0^2$, which corresponds to the threshold of the two-pion exchange spectrum. When we calculate $K_0(\nu)$ for real positive values of ν, we must evaluate the pricipal value integration in Eq.(5), however the direct numerical integration is extemely difficult because the "anti-bound state" causes the rapid change of $\delta_0(\nu)$, and it does not respect the ordinary threshold behavior except in the region of extremely small value of ν.

However the difficulty is bypassed, if we first calculate $K_0^{eff}(\nu)$. We introduce a polynomial $X_0^{eff}(\nu)$, which is the effective range expansion of $X_0(\nu)$ defined in Eq.(1). $h_0^{eff}(\nu)$

and $K_0^{eff}(\nu)$ are obtained from Eqs.(3) and (5) simply by substituting $X_0(\nu)$ by $X_0^{eff}(\nu)$. We point out that from Eq.(3) $h_0^{eff}(\nu)$ is a meromorphic function* on the k-plane, where $k = \sqrt{\nu}$. The upper half k-plane corresponds to the first sheet of ν. We claim

$$K_0^{eff}(\nu) = \sum_j \frac{Res(h_0^{eff}(\nu_j))}{(\nu - \nu_j)} \tag{7}$$

, where $Res(h_0^{eff}(\nu_j))$ are the residues of the poles, and the sum extends to all the poles on the first sheet of ν. This is shown by writing the Kantor amplitude in the form of the contour integration :

$$K_0(\nu) = -\frac{1}{2\pi i}\int_C d\nu' \frac{h_0(\nu')}{\nu' - \nu} \tag{8}$$

, where the contour C is given in Figure 1. When $X_0(\nu')$ is a polynomial of ν', such as $X_0^{eff}(\nu')$, then the singularities in the closed contour C are the poles of $h_0(\nu')$.† Therefore we can evaluate the contour integration by using the positions of the poles and their residues. The numerical evaluation of the correction to $K_0^{eff}(\nu)$ to obtain $K_0(\nu)$ is straightforward, because the spectral function of the principal value integration is $Im(h_0(\nu') - h_0^{eff}(\nu'))$, which does not involve the dominant effect of the "anti-bound state".

Finally, in order to guarantee the convergence of the integral representation Eq.(4) of the S-wave amplilude, we shall consider the once subtracted form of the Kantor amplitude $K_0^{(1)}(\nu)$, which is

$$K_0^{(1)}(\nu) \equiv \frac{K_0(\nu) - K_0(0)}{\nu}. \tag{9}$$

From the effective range parameters and the phase shift data, we can determine the precise values of the once subtracted Kantor amplitude $K_0^{(1)}(\nu)$ by

$$K_0^{(1)}(\nu) = \sum_j \frac{Res(h_0^{eff}(\nu_j))}{\nu_j(\nu - \nu_j)} + [\Delta K_0^{(1)}(\nu)]_R + [\Delta K_0^{(1)}(\nu)]_I \tag{10}$$

*Strictly speaking, this is true in the nonrelativistic approximation in which $\sqrt{m^2+\nu}$ in Eq.(3) is replaced by m.

†This is true for more general case, where $X_0(\nu')$ is a meromorphic function of $\sqrt{\nu'}$.

, where the corrections consist of two terms, which come from the real and imaginary part of $(h_0(\nu) - h_0^{eff}(\nu))$ respectively. They are

$$[\Delta K_0^{(1)}(\nu)]_R = Re\left(\frac{h_0(\nu) - h_0(0)}{\nu} - \frac{h_0^{eff}(\nu) - h_0^{eff}(0)}{\nu}\right) \tag{11}$$

, and

$$[\Delta K_0^{(1)}(\nu)]_I = \frac{P}{\pi}\int_0^\infty \frac{Im(h_0(\nu') - h_0^{eff}(\nu'))}{\nu'(\nu' - \nu)} d\nu' \tag{12}$$

, where P stands for the principal value integration.

3. The Kantor Amplitude with Coulomb Interaction

In this section, we consider the more practical case of the electric plus short range interactions. The electric interaction means the Coulombic interaction modified by the vacuum polarization effect, whose potential is

$$V^{vac}(r) = \lambda\frac{e^2}{r}\int_{4m_e^2}^\infty dt\, \frac{e^{-r\sqrt{t}}}{2t}\left(1 + \frac{2m_e^2}{t}\right)\sqrt{1 - \frac{4m_e^2}{t}} \tag{13}$$

, where m_e is the mass of the electron, and $\lambda = 2\alpha/3\pi = 1.549 \times 10^{-3}$. It is well-known that the quantity $X_0(\nu)$ which accepts the effective range expansion of ν is modified to

$$X_0(\nu) = \frac{C_0^2\sqrt{\nu}}{1 - \phi_0}[(1 + \chi_0)\cot\delta_0^E - \tan\tau_0] + me^2 h(\eta) + me^2 l_0(\eta) \tag{14}$$

, where

$$C_0^2 = \frac{2\pi\eta}{e^{2\pi\eta} - 1}\ ,\ with\ \ \eta = \frac{me^2}{2\sqrt{\nu}} \tag{15}$$

, and

$$h(\eta) = \eta^2\sum_{\ell=1}^\infty \frac{1}{\ell(\ell^2 + \eta^2)} - \log\eta - 0.57722\cdots. \tag{16}$$

τ_0 is the S-wave phase shift due to $V^{vac}(r)$, and three other functions χ_0 , ϕ_0 and $l_0(\eta)$ appeared in Eq.(14) are also small quantities of order of magnitude of the vacuum polarization potential. These functions are defined in [17]. Since these four functions are quite small, we shall neglect them, or treat them by perturbation, if it is necessary.

The S-wave amplitude $h_0(\nu)$ is also modified to

$$h_0(\nu) = \frac{1}{C_0^2}\frac{\sqrt{m^2+\nu}}{\nu}e^{i\delta_0^E(\nu)}\sin\delta_0^E(\nu) \tag{17}$$

, and which relates to $X_0(\nu)$ by

$$h_0(\nu) = \frac{\sqrt{m^2+\nu}}{X_0(\nu) - me^2h(\eta) - i\sqrt{\nu}C_0^2}. \tag{18}$$

When $X_0(\nu)$ is a polynomial of ν, inclusion of the Coulombic interaction causes small shifts of poles of $h_0(\nu)$ on the k-plane, which is related to ν by $k = \sqrt{\nu}$. However an additional series of poles and a logarithmic cut appear on the lower half k-plane, namely on the second sheet of the ν surface. On the other hand, the analytic structure of the first sheet of the ν surface remains the same.

The situation will become clear if we introduce κ by $\kappa = (e^{-i\pi}\nu)^{1/2}$, which maps the real negative axis of the first and the second sheet of the ν-surface to real positive axis and real negative axis of the κ plane respectively. Two terms in the denominator of Eq.(18) are rewritten as

$$-me^2h(\eta) - i\sqrt{\nu}C_0^2 = \kappa + me^2\{\log\frac{me^2}{2\kappa} - \psi(1+\frac{me^2}{2\kappa})\} \tag{19}$$

, where $\psi(z)$ is the digamma function and has poles at nonpositive integers of z. In between such poles, the denominator of $h_0(\nu)$ given in Eq.(18) vanishes. It is also worthwhile to notice that $h_0(\nu)$ is a real function of κ where $\nu = -\kappa^2$. Since no additional singularities appear in the first sheet of the ν-surface, when we include the Coulombic distortion of the scattering, we can use the same technique in computing the Kantor amplitude as that of the previous section.

There is another way to make the principal value integration manageable. We can arbitrarily subtract a function of zero-Kantor amplitude such as

$$f(\nu) = \frac{iC}{k+ia}\ , \quad with\ \ a > 0 \tag{20}$$

, or its generalization, where C is real and k is $(\nu)^{1/2}$. Since the pole stays on the second sheet of ν, its Kantor amplitude vanishes. However the spectral function does not vanish, rather $Imf(\nu) = C\sqrt{\nu}/(\nu+a^2)$. Therefore if we choose the position of the pole of $f(\nu)$ at

or close to the location of the pole of the "anti-bound state" of $h_0(\nu)$, then the spectral function of $(h_0(\nu) - f(\nu))$ becomes slowly varying function of ν, as long as we select the residue iC suitablly. At any rate, our aim is to calculate the Kantor amplitude $K_0(\nu)$ without reducing the precision of the input phase shift data.

4. Numerical Results of the Kantor Amplitude

In the previous two sections, we described the calculation of the Kantor amplitude from the phase shift data. In the data selection, following two points are important. Firstly, in order to observe possible singularity of the Kantor amplitude at $\nu = 0$, precise data in the very low energy region are required. Secondly, the input phase shift must be a smooth function of ν , because of the principal value integration involved in evaluating the Kantor amplitude. In the present paper, we shall analyse the energy dependent phase shift data of the Nijmegen group in the low energy region ($T_{lab} \leq 30Mev.$) [21]. Data of the intermediate energy region ($50 \leq T_{lab} \leq 350Mev.$) are those of the same group in a different paper [22]. In the higher energy region, the data of Arndt et.al.[18][19][20] are adopted, and which are used to estimate the contribution from the higher energy tail of the principal value integration of Eq.(12).

Since the low energy data of the Nijmegen group involve the precise and detailed table of $0.1Mev. \leq T_{lab} \leq 3.0Mev.$ region, we can use these data to obtain the effective range parameters of $X_0(\nu)$. However if the long range force is exerting, $X_0(\nu)$ is actually not analytic at $\nu = 0$, but rather it has a singularity of the form $C'\nu^2\log(\nu)$ for the case of the van der Waals potential of the Casimir-Polder type in paticular. Therefore we fit to the Nijmegen data in $T_{min} \leq T_{lab} \leq 3.0Mev.$ when we determine the effective range parameters c_j. Because the lowest precise experimental data analysed by the Nijmegen group are those at $T_{lab} \approx 0.35Mev.$, we consider three cases of $T_{min} = 0.25$, 0.30 and $0.35Mev.$, and the effective range curves $X_0^{eff}(\nu)$ of these fits are labeled as [.c25] , [.c30] and [.c35] respectively. In Table 1, the effective range parameters of the cubic fit

$$X_0^{eff}(\nu) = c_0 + c_1\nu + c_2\nu^2 + c_3\nu^3 \tag{21}$$

are tabulated. Three columns correspond to the different fits. $K_0^{eff}(\nu)$ has a real pole and a pair of complex poles on the first sheet of the complex ν surface, (see figure 1). The location of the poles and their residues are given in the same table.

By using Eq.(10), the Kantor amplitudes are calculated for the three sets of effective range parameters. In Table 2, the once subtracted Kantor amplitudes $K_0^{(1)}(\nu)$ minus the one-pion exchange contributions are tabulated, in which the π-N coupling constant is assumed to be $g^2/4\pi = 14.4$. In the same table, $X_0(\nu)$ are given for convenience. The last column is the error of the S-wave partial wave amplitude divided by ν obtained from the error of $\delta_0(\nu)$[22] , and which serves to estimate the errors of our Kantor amplitudes. As explained in section 2, $h_0^{eff}(\nu)$ is added and then subtracted in the process of the calculation of $K_0(\nu)$ in order to make the principal value integration manageable, therefore we may expect that $K_0(\nu)$ must be independent of the effective range parameters. However there are slight differences among the Kantor amplitudes given in columns 3 , 4 and 5 of Table 2. The differences come from our assumption that $(h_0(\nu) - h_0^{eff}(\nu)) = 0$ in $0 \leq T_{lab} \leq 3.0Mev.$. And these differences can be used in the estimation of the error of the Kantor amplitude in the very low energy region.

In figure 2 , $-\{K_0^{(1)}(\nu) - K_0^{(1),1\pi}(\nu)\}$ is plotted against T_{lab}. The curve is the column [.c30] of Table 2. The dash curve in the same figure is the one pole fit to the data in $50Mev. < T_{lab} < 240Mev.$ with a back ground constant, which will be explained in the next section. Figure 4 is the much expanded graph of the same quantity, in order to see the cusp at $\nu = 0$, the open circles and the closed circles in the figure correspond to columns [.c25] and [.c35] of Table 2, respectively. These figures already indicate that the once subtracted Kantor amplitude $K_0^{(1)}(\nu)$ has a huge cusp of attractive sign at $\nu = 0$, and which are very different from what are expected in the meson theory of the nuclear force. In the following three sections we shall analyse the Kantor amplitude to find the characteristic feature and the type of the extra force. After the searches of the minimum

of the chi square values, we shall find that the extra force is the van der Waals force with the strength of the strong interaction.

In the previous paper, the Kantor amplitude $K_{1,C}(\nu)$ of the central combination of the P-waves was calculated from the phase shift $\Delta_{1,C}$, which is shown in fig.4. The dash curve is the contrbution from the one-pion exchange. In fig.5, $-\{K_{1,C}(\nu) - K_{1,C}^{1\pi}(\nu)\}/\nu$ is plotted against T_{lab}. In the figure, the dash curve 2π is the two-pion exchange contribution, and we can already recognize the cusp of the attractive sign at $\nu = 0$, even in the P-wave Kantor amplitude. If we compare figures 3 and 5, differences of the accuracies of the curves are evident. Therefore we expect that we can extract much more information on the threshld behavior of the spectral function $A_t(4m^2, t')$ from our once subtracted Kantor amplitude of the S-wave compared to what was obtained from the analysis of the P-wane Kantor amplitude. In Section 6, we shall make chi square search to determine the parameters of the threshold behavior of $A_t(4m^2, t')$ with much higher accuracy.

5. Potential and the Pole Fit to the Kantor Amplitude

Let $A_t(s,t)$ be the spectral function of the t-channel of the scattering amplitude $A(s,t)$:

$$A(s,t) = \frac{1}{\pi}\int_{t_0}^{\infty} dt' \frac{A_t(s,t')}{t'-t} \pm \frac{1}{\pi}\int_{t_0}^{\infty} du' \frac{A_u(s,u')}{u'-u} \tag{22}$$

,where the u-channel spectral function A_u is the same as that of the t-channel, namely $A_u(s,*) = A_t(s,*)$. The plus and minus signs between the integrations of Eq.(22) correspond to the spin singlet and the spin triplet states respectively. The nuclear potential of the central combination $V(r)$ is related to the spectral function by a kind of the Laplace transformation:

$$V(r) = -\frac{1}{\pi m^2}\frac{1}{r}\int_0^{\infty} dt' A_t(s,t') e^{-r\sqrt{t'}}. \tag{23}$$

In Eq.(23), s is set equal to its threshold value $4m^2$ in order to avoid the energy dependency of the potential $V(r)$, with the understanding that the potential can be useful when the

kinetic energy is much smaller than the energy of the rest mass, namely $\nu \ll 2m^2$. The coefficient appeared in front of the integration of Eq.(23) can be checked by making the Fourier transformation $\int d^3r \exp[-i\vec{K}\cdot\vec{r}]\cdots$ of Eq.(23) to obtain Eq.(22), in which the momentum transfer vector $\vec{K}$ relates to the Mandelstam variable t by

$$t = -|\vec{K}|^2 = -2\nu(1-\cos\theta). \tag{24}$$

The second term of the r.h.s. of Eq.(22) is obtained by simply replacing t by u, where $u = -2\nu(1+\cos\theta)$.

On the other hand, the partial wave projection of Eq.(22) results in

$$h_\ell(\nu) = \frac{1}{2\nu}\int_{t_0}^{\infty} dt' A_t(s,t') Q_\ell(1+\frac{t'}{2\nu}) \pm (\ \textit{crossed term}\ ) \tag{25}$$

The left hand cut of $h_\ell(\nu)$ comes from the cut of $Q_\ell(z)$, the location of which is $-1 \le z \le 1$, whereas the right hand cut, namely the unitarity cut, comes from the s-cut of the spectral function $A_t(s,t')$. To obtain the Kantor amplitude $K_\ell(\nu)$, we must set s appeared in $A_t(s,t')$ in Eq.(25) equal to $4m^2$. Therefore the potential and the Kantor amplitude are related by Eqs.(23) and (25) with the mediation of the spectral function $A_t(4m^2,t')$. Our problem is to determine $A_t(4m^2,t')$ from the data of the once subtracted Kantor amplitude $K_0^{(1)}(\nu)$:

$$K_0^{(1)}(\nu) = \int_{t_0}^{\infty} dt' A_t(4m^2,t')\frac{1}{\nu}[\frac{1}{4\nu}\log(1+\frac{4\nu}{t'}) - \frac{1}{t'}]. \tag{26}$$

Before we determine the spectral function $A_t(4m^2,t')$, let us try the one-boson exchange type fits to $K_0^{(1)}(\nu) - K_0^{(1),1\pi}(\nu)$:

$$A_t(4m^2,t') = \sum_j \tilde{g}_j^2 \cdot t'^2\, \delta(t'-m_j^2). \tag{27}$$

1. One pole fit to the data of $50Mev. \le T_{lab} \le 240Mev.$ is carried out. Chi square minimum $(0.35)^2$ appears at $m_1^2 = 9.48$ in the unit of the neutral pion mass.[‡] The coeffient $\tilde{g}_1^2$ is 1.91. The curve of the one-pole fit is shown in fig.2 and 3 of Section 4 as the dash curve. This pole corresponds to the σ meson exchange in the one-boson exchange model (OBE) . Deviation of the OBE fit from our Kantor amplitude in the very low energy region is clearly seen.

2. One pole fit to the low energy data of $T_{lab} < 60Mev.$ is made. Chi square minimum $(2.22)^2$ occurs at $m_1^2 = 2.05$ with coefficient $\tilde{g}_1^2 = 1.62$.

3. Two-pole fit to the wide range data of $T_{lab} < 250Mev.$ is done. The chi square attains its minimum values of $(1.29)^2$ at $m_1^2 = 0.78$ and $m_2^2 = 15.3$, whose coefficients are $\tilde{g}_1^2 = 0.96$ and $\tilde{g}_2^2 = 1.66$ respectively.

[‡]Hereafter we shall use the mass of the neutral pion as the unit of the energyy, except when it is explicitely stated otherwise

These pole fits indicate that results are different from what is expected in the meson theory of the nuclear force. Since in the meson thory, the nuclear force is due to the exchanges of a pion and a set of pions. In our data in Table 2, the one-pion exchange contribution was already subtracted. Therefore the nearest spectra must be due to the exchanges of two-pion states, whose threshold is $t = 4$. Our fits, especially the fit (3), require an effective pole around $\sqrt{t} \approx 1$, whereas the location of the nearest effective pole of the meson theory must be much larger than $\sqrt{t} = 2$. A new mechanism other than the exchanges of mesons must exist, which produces a longer range nuclear force compared to the force arising from the two-pion exchange. In the next section we shall determine the type and strength of such a new force.

6. Threhold Behavior of the Spectral Function

In Section 5, we observed that the once subtracted Kantor amplitude minus the one-pion exchange contribution, namely $K_0^{(1)}(\nu) - K_0^{(1),1\pi}$, cannot be fitted by the spectral function arising from the exchanges of two or more pions. Rather it requires an extra meson whose mass is smaller than the pion mass. However such a meson is not observed in Nature. Therefore we must consider other possibilities. In order to understand the

characteristic feature of the extra force more closely, we would like to determine the extra spectral function $A_t(4m^2, t')$ for small t'. We are especially interested in the threshold behavior of such a spectral function at $t' = 0$. It must be remembered that in the meson theory of the nuclear force, such a spectral function is strictly zero in $t' \leq 4$.

Equation (23) indicates that $rV(r)$ is the Laplace transformation of the spectral function $A_t(4m^2, t')$ with respect to the variable $\sqrt{t'}$. Therefore the asymptotic form of $V(r)$ for large r is determined solely by the threshold behavior at $t' = 0$ of the spectral function. On the other hand, from Eq.(26), the singularity of the once subtracted Kantor amplitude $K_0^{(1)}(\nu)$ at $\nu = 0$ is also determined by the threshold behavior of the same function $A_t(4m^2, t')$. In particular, when the spectral function is $A_t = \pi C' t'^{\gamma}$, then the potential becomes

$$V(r) = -C' \frac{2\Gamma(2\gamma+2)}{m^2} \frac{1}{r^{2\gamma+3}} \tag{28}$$

,whereas the threshold behavior of the once subtracted Kantor amplitude is

$$K_0^{(1)}(\nu) = \begin{cases} C''\nu^{\gamma-1} + \cdots & (\gamma \neq integer) \\ C''\nu^{\gamma-1}\log\nu + \cdots & (\gamma = integer) \end{cases} \tag{29}$$

, where C'' is proportional to C'.

In general, the asymptotic behvior of the potential and the threshold singularity of the Kantor amplitude at $\nu = 0$ is related each other through the spectral function. In particular, the van der Waals potential of the Casimir-Polder type, whose asmptotic form is $V(r) \sim -C/r^7$, corresponds to $\gamma = 2$ of the threshold behavior of the spectral function, and the singularity is $K_0^{(1)}(\nu) = C''\nu\log\nu + \cdots$. In the same way, the potential of the London type corresponds to $\gamma = 1.5$, and the threshold behavior is $K_0^{(1)}(\nu) = C''\sqrt{\nu} + \cdots$.

In order to find the power γ of the threhold behavior from our once subtracted Kantor amplitude, the chi square minimum is searched with the spectral function of the form :

$$A_t(4m^2, t') = \pi C' t'^{\gamma} e^{-\beta t'} \tag{30}$$

in which the exponential factor is necessary to make the integration of Eq.(26) convergent, and the parameter β must be small compared to the size squared of the composite system. The projection factor appeared in the integrand of Eq.(26) is

$$\frac{1}{\nu}\{\frac{1}{2\nu}Q_0(1+\frac{t'}{2\nu}) - \frac{1}{t'}\} = \frac{1}{\nu}\{\frac{1}{4\nu}\log(1+\frac{4\nu}{t'}) - \frac{1}{t'}\} \tag{31}$$

for the once subtracted Kantor amplitude, and which dampes as $(4\nu/t')^{-2}$ for large t'. Because of such damping property of the projection factor in Eq.(26), the value of the spectral function $A_t(4m^2, t')$ in $t' \gtrsim 4\nu$ does not sensitively relate to $K_0^{(1)}(\nu)$. Therefore when we fit to $K_0^{(1)}(\nu)$ in the domain of $0 < \nu < \nu_{max}$ to extract information about $A_t(4m^2, t')$, we can not expect to obtain precise information on the spectral function in the region of $t' \gtrsim 4\nu_{max}$. In this paper we are going to analyse the Kantor amplitude in $0 \leq T_{lab} \leq 30 Mev.$, namely in $0 \leq \nu \leq 0.77$, we can expect to obtain reliable information about the spectral function $A_t(4m^2, t')$ only in $0 < t' < 3$.

In fig.6, on the γ-β plane the chi values per data point $\chi(\gamma, \beta)$ are plotted as the contour curves. Since the fitting function of Eq.(30) involves three free parameters, namely C' , γ and β, the minimun value χ of the function $\chi(\gamma, \beta)$ is obtained by varying the coefficient C' with γ and β fixed. Because the differences of the Kantor amplitudes of columns 3, 4 and 5 of Table 2 are small, we analyse only the data of column 4, namely [.c30] , and in the chi square search we used the error estimation of $K_0^{(1)}(\nu)$

$$\Delta(K_0^{(1)}(\nu)) = \begin{cases} 0.005/\sqrt{\nu} \\ 0.02\,, \end{cases} \quad \text{if } \nu < 0.0625 \ . \tag{32}$$

This error estimation was already used in the pole fits in section 5. We carried out the chi square fit to the once subtracted Kantor amplitude in various domains $[\,0, T_{max}]$, and the fig.5 is an example for $T_{max} = 26$ Mev. among such fits. When we change the fitted domains, the graphs of the contour curves also change slowly, however there remains a pattern in common, that is on the γ-β plane, there is a narrow trench of $\chi(\gamma, \beta)$. Therefore it is convinient to introduce a function $\chi_{min}(\gamma)$:

$$\chi_{min}(\gamma) = \min_{\beta} \ \chi(\gamma, \beta). \tag{33}$$

Curves in fig.7 are the plots of $\chi_{min}(\gamma)$ against γ for different fitted domains $[\,0, T_{max}]$. In the figure, values of T_{max} are witten in the unit of Mev.. We can observe in the figure that as the fitted domain shrinks the bottom of the curve becomes shallower and therefore

the minimum point γ cannot be sharply determined. However this fact is not so surprising, because the shrink of the fitted domain means the decrease of the number of the data to be fitted, while the number of the free parameters remains the same. What is really important is that the minimum point γ increases slowly as the fitted domain shrinks. In section 7, physical meaning of such phenomena will be considered.

7. Van der Waals Potential and the Transition from the London to the Casimir-Polder Type

The chi square search in the previous section indicates that the power γ of the threshlod behavior introduced in Eq.(30) turns out to be $1.55 < \gamma \lesssim 2.$, and the coefficient C' is positive. From these results, the asymptotic behavior of the potential $V(r) \approx -C/r^{\alpha}$ is determined. Equations (23) and (28) indicate that the sign of the potential is attractive, and $6.1 < \alpha \lesssim 7$. Before we conclude that the extra force is the van der Waals force, it is desirable to examine the transition from the London type ($\alpha = 6$) to the Casimir-Polder type ($\alpha = 7$), which is expected in the general theory of the van der Waals interaction.[24] There is a characteristic length r_c, which is around the Compton wave length of the excitation energy to the states which are accesible from the ground state by the absorption of a vector particle. For our case of the proton, using the mass difference of the Δ-particle and the nucleon, $r_c \approx 0.6fm$.. In the region $r \gg r_c$, the potential behaves as the Casimir-Polder type, whereas the region $r_0 \ll r \ll r_c$ is that of the London type, where r_0 is the size of the composite particle.

The neighborhood of $r = r_c$ belongs to the transient region. In terms of the spectral function, t_c, which is the excitaion energy squared and separates the two types of spectra, is equal to 4.8 . Therefore when we fit to the Kantor amplitude in the relatively low energy domain, only the spectral function of the Casimir-Polder region contributes, because the factor in the integrand of Eq.(26) damps as $(4\nu/t')^2$. As the fitted domain $[0, T_{max}]$ expands, the contribution from the London region of the spectrum becomes more and

more important, and the power γ of the minimun point of χ must approaches to 1.5 . In fig.7, we can see such a behavior of the moving bottom point.

In Table 3, the dependency of γ , the minimum point of the chi value, on the fitted domain $[0, T_{max}]$ is given. The first column is the fitted domain. Columns 2, 3 and 4 are γ, β and C' respectively. In fig.8, γ , at which $\chi_{min}(\gamma)$ attains its minimum value $\chi_{[min]}$, is plotted against T_{max}, the upper bound of the fitted domain. The dashed curves are the γ's at which χ are 5 per cent larger than the minimum value of $\chi_{min}(\gamma)$, namely the solutions of

$$(1 + 0.05)\chi_{[min]} = \chi_{min}(\gamma). \tag{34}$$

For small shift, the solution of Eq.(34) is $\Delta\gamma = (\chi''_{min}/2\chi_{min})^{-1/2}\sqrt{0.05}$, and the coefficient of the right hand side is tabulated in column 5 of Table 3. The last column is $\chi_{[min]}$.

Figure 8 shows that γ increases slowly as the domain $[0, T_{max}]$ shrinks, and which is consistent with the transition from the London type to the Casimir-Polder type of the van der Waals interaction.[24] However at present, data are not accurate enough to confirm that γ approaches to 2 as T_{max} goes to zero, or in terms of the potential the relevant region r tends to infinity. From Table 3, the coefficient C' of the spectral function at $\gamma = 2$ is

$$C' = 0.483 \quad for \;\; \gamma = 2 \tag{35}$$

, which is to be compared with $C' = 0.64$ obtained from the analysis of the P-wave phase shift in the previous paper.[12] In view of the lower accuracy of the P-wave phase shift data, these values are not inconsistent. If we use Eq.(28), the coefficient C of $V(r) \sim -C/r^7 + \cdots$ is

$$C = 2.40 \tag{36}$$

in the unit of the Compton wave length of the neutral pion, and which will become an important constant when we construct a new nuclear potential based on the strong van der Waals interaction as well as the meson exchanges. It is interestig to see that the spectral function of Eq.(30) has a peak at $t' = \gamma/\beta$, and which is numerically around 20 if we take

average of data in $7Mev. < T_{max} < 30Mev.$ of Table 3 , where the region stays away of the Casimir-Polder region. The peak at $\sqrt{t_{peak}} \approx 600Mev.$ gives another interpretation of the fictitious σ-meson in the one boson exchange model of the nuclear potential. Investigations of this direction and the potential making will appear in a separate paper.

It is desirable to observe directly the effect of the strong long range force as the difference of the interference pattern with the Coulombic peak from what is expected in the case of the short range nuclear potential. The most favorable incident energy is around $T_{lab} = 15Mev. \sim 30Mev.$, and the required precision of the measurements of the angular distribution of the cross section is 0.2% . Since we are going to observe the singularity at $t = 0$, data of the smaller angular region are necessary, and the ordinary angular domain of the data taking, which is usually $12° \leq \theta_{lab} \leq 168°$, is not sufficient. Details will be given also in a separate paper.

In general, as the incident energy T_{lab} decreases the the required precision of the measurements increases, although the requirement on the angular domain becomes some what less severe. As an extreme example, we shall mention the p-p scattering in 0.35 Mev.$< T_{lab} <$ 2 Mev.. In such a low energy scattering, data are usually fitted by the amplitude which is the sum of the terms of Coulomb, vacuum polarization and the S-wave plus P-wave terms arising from the short range potential. The term of the vacuum polarization is not negligible, since it is around 0.5% of the Coulomb term. If P-wave phase shift $\Delta_{1,C}(\nu)$ is brought from the phase shift of higher energy, only free parameter is $\delta_0(\nu)$. However if there is the van der Waals interaction with the strength determined in this paper, the angular distribution of the cross section cannot be reproduced by varying the single free parameter $\delta_0(\nu)$. Rather, roughly speaking, the effect of the attractive van der Waals force is to reduce the repulsive term of the vacuum polarization in some extent.

Wassmer and Mühry[16] claimes that their data of the p-p cross section at $T_{lab} = 1Mev.$ measured with accuracy of 0.1% can be fitted well if the term of the vacuum polarization is reduced by a factor 0.4 . However the situation is not settled well, since the angular distrbution of the cross section at the same energy measured by Thomann, Benn and

Münch[14] can be fitted without reducing the vacuum polarization term.

8. Discussions and Comments

In the present paper, it is shown by analysing the once subtracted S-wave Kantor amplitude that the nuclear potential must involve the long range potential whose asymptotic form is $V(r) \sim -C/r^{\alpha}$. The power α is determined, which turns out $6.1 < \alpha \lesssim 7.$, and moreover α increases slowly from 6.1 to 7 as the relevant value r of the potential increases. We can regard the phenomenon as the transition from the London type ($\alpha = 6$) to the Casimir-Polder type ($\alpha = 7$) of the van der Waals interaction. It is important to emphasize that the long range force is not a small correction to the short range force in the nuclear force. Because the total value of the once subtracted Kantor amplitude of the S-wave at $\nu = 0$ is -12.02, while the contribution from the one-pion exchange is -7.20 , and the remainder is -4.82 , which is tabulated in the first line of Table 2. We analysed the remainder by assuming that it came from the spectral functions of the long range interaction plus the short range interactions other than the one-pion exchange.

It is instructive to consider why the long range force of the nuclear force has escaped our observation for such a long time, when the portion of the contribution from such an extra force is as large as around 40 % of the nuclear phenomena. When the precisins of the data are not very high, the pole of the σ-particle or in general the spectral function starting at $t' = 4$, plays the role of the spectrum of the long range force, and reproduces approximately well the required amplitude. Therefore in such a case, in order to observe the effects of the long range force in a clear-cut way, we must calculate the spectrum of the two-pion exchanges and subtract it. Such situations are common in the hadron-hadron scattering, where the measurements with a few per cent error are regarded as the ' accurate experiments '. However the nucleon-nucleon scatterings are prominent exceptions. Especially, the low energy data of the proton-proton scatterings attain the accuracy of 0.1% $\sim$ 0.2%, and therefore it is not necessary to subtract the contributions

from the two-pion exchanges, in order to observe the long range force. It is sufficient to subtract only the singularity of the one-pion exchange.

The most of the information of the low energy scattering with high precision are cocentrated in the phase shifts of the S-wave $\delta_0^E(\nu)$, and to some extent in $\delta_{1,C}(\nu)$, the central combination of the P-wave phase shifts. Since to recognize the long range force is to observe a new singularity at $\nu = 0$ in the partial wave amplitudes $h_\ell(\nu)$, we must prepare the wide analytic domain by eliminating the known near-by singularities. The nearest left hand singularity is that of the one-pion exchange amplitude $h_\ell^{1\pi}(\nu)$. The eliminations of the unitarity cut of $h_\ell(\nu)$, which starts at $\nu = 0$, are performed by introducing the effective range function $X_\ell(\nu)$ of Eq.(1). However because $X_\ell(\nu)$ is essentially the invese of the partial wave amplitude $h_\ell(\nu)$, we can not eliminate the one-pion singularity from $X_\ell(\nu)$ by using the mass and $g^2/4\pi$ of the π-N coupling alone. Therefore the use of the Kantor amplitude of Eq.(5) is essential. The numercal evaluation of the Kantor amplitude of the P-wave is straightforward, because the principal value integration is only the small correction to $Re(h_1(\nu))$ due to the threshold behavior of the phase shifts of the higher partial waves. On the contrary, in the evaluation of the S-wave Kantor amplitude, especially of the once subtracted Kantor amplitude, the numerical calculation of the principal value integration is prohibitive, because of the anti-bound state of the S-wave. To circumvent such difficulty, we have to use the technique explained in section 2. After we can overcome these hurdles, we obtain the once subtracted Kantor amplitude of the S-wave, where we can see the completely different scenary from what is expected in the meson theory of the nuclear force.

Let us turn to the universality. If the van der Waals interaction is universal[25], we must expect to observe such forces in other types of hadron-hadron scatterings. However at present accuracies of measurements of such scatterings are much lower compared to the p-p scattering. Moreover since the scattering lengths are not determined with high accuracy, we must use the data of the P-waves. I analysed the pion-nucleon and pion-pion scatterings. However because of the accuracy, I had to separate also the spectral

function arising from the two-pion exchanges in order to make it easy to observe the effect of the van der Waals interaction. By assuming $\gamma = 2$, the coefficients $C'_{\pi\cdot N}$ and $C'_{\pi\cdot\pi}$ were determined, and they were 0.16 and 0.031 respectively[26, 27]. These coefficients must satisfy the factorizability condition with the coefficient of the N-N scattering given in Eq.(35), namely

$$(C'_{\pi\cdot N})^2 = C'_{N\cdot N}C'_{\pi\cdot\pi}. \tag{37}$$

However at present there is 25% discrepancy between the numerical values of the right and the left hand sides of the equation.

Finally, when the strong van der Waals force appears in the hadron-hadron interaction, and the van der Waals force arises as the secondary force of the basic Coulomb interaction between the constituent particles, it is tempting to regard the 'charge' of the basic Coulomb force as the colour. However after the strength C of the van der Waals potetial is known, there is a lower bound of the coupling constant $^*e^2$ of the basic Coulomb force, which is around 10. Therefore the coupling constant of the QCD seems to be too small. On the other hand Dirac's magnetic monopole, whose coupling constant is $^*e^2 = 137/4$, will be a good candidate[28]. Details of such estimation will be published in a separate paper.

Acknowledgement

The auther would like to thank Dr.K.Nojima for discussions and his enlightening comments.

Figure Captions

Fig.1 The contour C of the integration on ν' in Eq.(8).

Fig.2 $-\{K_0^{(1)}(\nu) - K_0^{(1),1\pi}(\nu)\}$ is plotted against T_{lab}. The curve is the column [.c30] of Table 2. The dash curve is the one-pole fit to the data in $50Mev. < T_{lab} < 240Mev.$ with an additional back ground constant.

Fig.3 Amplified graphs of the low energy region in the box of fig.2. are displayed. The curve is [.c30] of Table 2, whereas the the open circles and the closed circles are the column [.c25] and [.c35] of the Table 2, respectively. The dash curve is the same as that of fig.2. The cusp at $\nu = 0$ indicates the long range force with attractive sign.

Fig.4 The central combination $\Delta_{1,C}$ of the P-wave phase shifts is plotted against T_{lab}. Open squares are Wisconsin data,[8] open circles are Kyoto data[9] and closed circles are Minesota data.[10] The closed square and closed triangle are data of [6] and [7] respectively. Dash curve is the one-pion exchange contribution (OPE).

Fig.5 The P-wave Kantor amplitudes with error bars are shown, namely $\{K_{1,C}(\nu) - K_{1,C}^{1\pi}(\nu)\}/\nu$ are plotted against T_{lab}. The graphs, especially the sizes of the errors, must be compred with the graphs of the same quantity of the once subtracted Kantor amplitude of the S-wave displayed in fig.3 .

Fig.6 Contours of chi per data point on the γ-β plane. $\{K_0^{(1)}(\nu) - K_0^{(1),1\pi}(\nu)\}$ is fitted using the spectral function of the form $A_t(4m^2, t') = \pi C' t'^{\gamma} e^{-\beta t'}$. The energy domain of the fitted data are $0 < T_{lab} < 26Mev.$.

Fig.7 Curves of $\chi_{min}(\gamma)$ are plotted against γ. Curves correspond to different fitted domains $[0, T_{max}]$. T_{max} are 26 Mev., 18 Mev., 12 Mev., 8 Mev. and 4.5 Mev. respectively. We can observe that the minimum point γ increases slowly as the fitted domain shrinks.

Fig.8 γ of the minimum point is plotted against T_{max}, the upper bound of the fitted domain $[0, T_{max}]$. The dash curves are the values of γ at which $\chi_{min}(\gamma)$ are 5% larger compared to the minimum value $\chi_{[min]}$ to show the uncertainty of γ.

Table Captions

Table 1 Table of the coefficients c_j of the effective range expansion $X_0(\nu) = \sum_{j=0}^{3} c_j \nu^j$ of the S-wave amplitude. $K_0^{eff}(\nu)$ has a real pole and a pair of complex poles. The location ν_P and the residue r_P of the real pole, and also $\nu_{P'}$ and $r_{P'}$ of the complex pole are tabulated. Three columns correspond to different effective range fits which are obtained by fitting to the data in different domains $T_{min} \leq T_{lab} \leq 3.0Mev.$. T_{min} are 0.25 , 0.30 and 0.35 Mev. , and whose labels are [.c25] , [.c30] and [.c35] respectively.

Table 2 The first column is the incident energy T_{lab} in Mev.. The second column is $X_0(\nu)$. The third, fourth and fifth columns are $\{K_0^{(1)}(\nu) - K_0^{(1),1\pi}(\nu)\}$, in which the adopted effective range parameters are obtained by fitting to the data in $0.25 \leq T_{lab} \leq 3.0$, $0.30 \leq T_{lab} \leq 3.0$ and $0.35 \leq T_{lab} \leq 3.0$ in Mev. respectively. The sixth column is the error of $h_0(\nu)/\nu$, and which is useful to estimate the error of the once subtracted Kantor amplitude, namely $\Delta K_0^{(1)}(\nu)$.

Table 3 The minimum points (γ, β) of $\chi(\gamma, \beta)$ are tabulated for various fitted domains $(0, T_{max})$. The first column is the fitted domain. The second, third and fourth columns are γ , β and the coefficient C' respectively at the minimum point. The fifth column is $(\chi''_{min}(\gamma)/2\chi_{min}(\gamma))^{-1/2}$, which is proportional to the uncertainty of γ. The last column is the minimum value of chi $\chi_{[min]}$. We can observe that as the fitted domain shrinks γ moves slowly from the London value ($\gamma = 1.5$) to the Casimir-Polder value ($\gamma = 2.0$).

References

[1] H. Yukawa , Proc. Phys. Math. Soc. Japan **17** , 98 , (1935)

[2] N.C.Kim, J.W.Durso and K. Holinde , Phys. Rev. **C 49** , 2355 , (1994)

[3] R.Machleidt, K. Holinde and Ch. Elster , Phys. Rep. **149** , 1 , (1987)

[4] D. Plümper, J. Flender and M. F. Gari , Phys. Rev. **C49** , 2370 , (1994)

[5] J. Heidenbauer, K. Holinde and A. W. Thomas , Phys. Rev. **C49** , 2331 , (1994)

[6] L. H. Johnston and D. E. Young, Phys. Rev. **116** , 989 , (1959)

[7] N. Jarmie, J. H. Jett, J. L. Detch Jr. and R. L. Hutson , Phys. Rev. **C3** , 10 , (1971)

[8] D. J. Knecht, P. F. Dahl and S. Masselt , Phys. Rev. **148** , 1031 , (1966)

[9] K. Imai, K. Nishimura, N. Tamura and H. Sato , Nucl. Phys. **A246** , 76 , (1975)

[10] P. M. Hegland, R. E. Brown, J. S. Lilley and J. A. Koepke , Phys. Rev. Lett. **39** , 9 , (1977)

[11] T. Sawada , Phys. Lett. **43B** , 517 , (1973)

[12] T. Sawada , Nucl. Phys. **B71** , 82 , (1974)
T. Sawada , Prog. Theor. Phys. **59** , 149 , (1978)

[13] M. S. Sher, P. Signell and L. Heller , Ann. Phys. **58** , 1 , (1970)

[14] Ch. Thomann, J. E. Benn and S. Münch Nucl. Phys. **A303** , 457 , (1978)

[15] P. B. Kantor , Phys. Rev. Lett. **12** , 52 , (1964)

[16] von H. Wassmer and M ühry , Helv. Phys. Acta **46** , 626 , (1973)

[17] L. Heller , Phys. Rev. **120** , 627 , (1960)

[18] R. A. Arndt, L. D. Roper, R. A. Bryan, R. B. Clark, B. J. DerWest and P. Signell , Phys. Rev. **D28** , 97 , (1983)

[19] R. A. Arndt, J. S. Hyslop III and L. D. Roper, Phys. Rev. **D35** , 128 , (1987)

[20] R. A. Arndt, L. D. Roper, R. L. Workman and M. W. McNaughton , Phys. Rev. **D45** , 3995 , (1992)

[21] J.R. Bergervoet, P.C. van Campen, W.A. van der Sanden and J.J. de Swart , Phys. Rev. **C38** , 15 , (1988)

[22] V.G.J. Stoks , R.A.M. Klomp , M.C.M. Rentmeester and J.J. de Swart , Phys. Rev. **C48** , 792 , (1993)

[23] O. Dumbrajs, R. Koch, H. Pilkuhn, G. C. Oades, H. Behrens, J. J. DeSwart and P. Kroll , Nucl. Phys. **B216** , 277 , (1983)

[24] G. Feinberg and J.Sucher , Phys. Rev. **139B** , 1619 , (1965)
G. Feinberg and J. Sucher , Phys. Rev. **A2** , 2395 , (1970)
J. Sucher , Cargése Lecture in Physics vol.6 , ed. M. Lévy , Gordon and Breach (1977)

[25] T. Sawada , Phys. Lett. **B100** , 50 , (1981)

[26] T. Sawada , Nuovo Cimento **62A** , 207 , (1981)

[27] T. Sawada , Prog. Theor. Phys. **63** , 2016 , (1980)
T. Sawada , Phys. Lett. **B225** , 291 , (1989)

[28] P. A. M. Dirac , Proc. R. Soc. London **A133** , 60 , (1931)
J. Schwinger , Science **165** ,757 , (1969)
A. O. Barut , Phys. Rev. **D3** , 1747 , (1971)
T. Sawada , Phys. Lett. **B43** , 517 ,(1973)

Table 1.

curve	[.c25]	[.c30]	[.c35]
Fitted region	$.25 \leq T_{lab} \leq 3.0$ $(Mev.)$	$.30 \leq T_{lab} \leq 3.0$ $(Mev.)$	$.35 \leq T_{lab} \leq 3.0$ $(Mev.)$
c_0	0.187156	0.187161	0.187162
c_1	0.95666	0.95627	0.95621
c_2	−0.3482	−0.3389	−0.3376
c_3	1.0842	1.0174	1.0079
ν_P	−0.53315	−0.54146	−0.54268
r_P	4.2848	4.3653	4.3772
$\Re(\nu_{P'})$	0.62701	0.64209	0.64433
$\Im(\nu_{P'})$	−0.84972	−0.87519	−0.87899
$\Re(r_{P'})$	−0.80053	−0.82409	−0.82759
$\Im(r_{P'})$	2.5913	2.6155	2.6190

Table 2.

$T_{lab}(Mev.)$	$X_0(\nu)$	$K_0^{(1)}(\nu) - K_0^{(1),1\pi}(\nu)$			$\Delta h_0(\nu)/\nu$
		[.c25]	[.c30]	[.c35]	
0	.18716	−4.8701	−4.8238	−4.8172	...
1	.21158	−4.6629	−4.6344	−4.6303	$.102 + i.223$
2	.23610	−4.4856	−4.4693	−4.4670	$.061 + i.168$
3	.25950	−4.3394	−4.3293	−4.3279	$.027 + i.121$
4	.28315	−4.2302	−4.2226	−4.2215	$.001 + i.083$
5	.30665	−4.1402	−4.1343	−4.1335	$-.019 + i.053$
6	.33008	−4.0502	−4.0453	−4.0446	$-.028 + i.034$
7	.35344	−3.9752	−3.9710	−3.9704	$-.028 + i.026$
8	.37677	−3.9084	−3.9047	−3.9042	$-.022 + i.026$
9	.40008	−3.8447	−3.8414	−3.8410	$-.014 + i.027$
10	.42344	−3.7858	−3.7829	−3.7825	$-.010 + i.026$
12	.47017	−3.6810	−3.6785	−3.6782	$-.007 + i.018$
14	.51702	−3.5886	−3.5865	−3.5863	$-.005 + i.014$
16	.56406	−3.5053	−3.5034	−3.5032	$-.004 + i.012$
18	.61135	−3.4292	−3.4275	−3.4273	$-.003 + i.011$
20	.65899	−3.3589	−3.3574	−3.3572	$-.003 + i.011$
22	.70704	−3.2933	−3.2918	−3.2916	$-.002 + i.011$
24	.75559	−3.2305	−3.2291	−3.2289	$-.002 + i.011$
26	.80471	−3.1707	−3.1694	−3.1692	$-.001 + i.009$
28	.85449	−3.1126	−3.1113	−3.1111	$-.000 + i.008$
30	.90502	−3.0508	−3.0496	−3.0495	$.0001 + i.0073$
35	1.0379	−2.9226	−2.9215	−2.9214	$.0007 + i.0058$
40	1.1766	−2.8235	−2.8224	−2.8223	$.0008 + i.0052$
45	1.3218	−2.7391	−2.7382	−2.7381	$.0008 + i.0048$
50	1.4735	−2.6650	−2.6642	−2.6641	$.0009 + i.0043$
60	1.7949	−2.5299	−2.5293	−2.5292	$.0014 + i.0030$
70	2.1749	−2.4075	−2.4070	−2.4069	$.0016 + i.0024$
80	2.5366	−2.2962	−2.2958	−2.2957	$.0016 + i.0022$
90	2.9706	−2.1948	−2.1944	−2.1943	$.0016 + i.0021$
100	3.459	−2.1019	−2.1015	−2.1015	$.0016 + i.0019$
120	4.662	−1.9396	−1.9393	−1.9392	$.0018 + i.0015$
140	6.296	−1.8009	−1.8006	−1.8006	$.0019 + i.0012$
160	8.66	−1.6803	−1.6801	−1.6800	$.0020 + i.0010$
180	12.4	−1.5742	−1.5740	−1.5739	$.0019 + i.0007$
200	19.3	−1.4797	−1.4796	−1.4795	$.0018 + i.0004$
220	36.1	−1.3951	−1.3949	−1.3949	$.0016 + i.0002$
240	142.	−1.3185	−1.3184	−1.3184	$.0015 + i.0001$

Table 3.

fitted domain in Mev.	min. point γ	β	coefficient C'	$\sqrt{\frac{2\chi_{min}(\gamma)}{\chi''_{min}(\gamma)}}$	min. value $\chi[min]$
(0. , 4.0)	2.198	.2811	.5777	.7964	.2209
(0. , 4.25)	2.048	.2173	.5048	.6999	.2696
(0. , 4.5)	1.938	.1740	.4556	.6354	.3080
(0. , 5.0)	1.815	.1298	.4049	.5218	.3386
(0. , 6.0)	1.777	.1172	.3902	.3924	.3125
(0. , 7.0)	1.759	.1116	.3842	.3140	.2902
(0. , 8.0)	1.711	.0976	.3691	.2632	.2923
(0. , 9.0)	1.681	.0893	.3602	.2261	.2885
(0. , 10.)	1.663	.0848	.3555	.1971	.2795
(0. , 12.)	1.633	.0773	.3479	.1596	.2709
(0. , 14.)	1.605	.0709	.3418	.1388	.2745
(0. , 16.)	1.584	.0662	.3376	.1243	.2785
(0. , 18.)	1.569	.0632	.3349	.1120	.2776
(0. , 20.)	1.559	.0612	.3334	.1012	.2720
(0. , 22.)	1.554	.0602	.3326	.0915	.2627
(0. , 24.)	1.556	.0606	.3328	.0841	.2528
(0. , 26.)	1.566	.0623	.3339	.0842	.2615
(0. , 28.)	1.581	.0652	.3355	.0967	.3068
(0. , 30.)	1.616	.0716	.3385	.1605	.5036

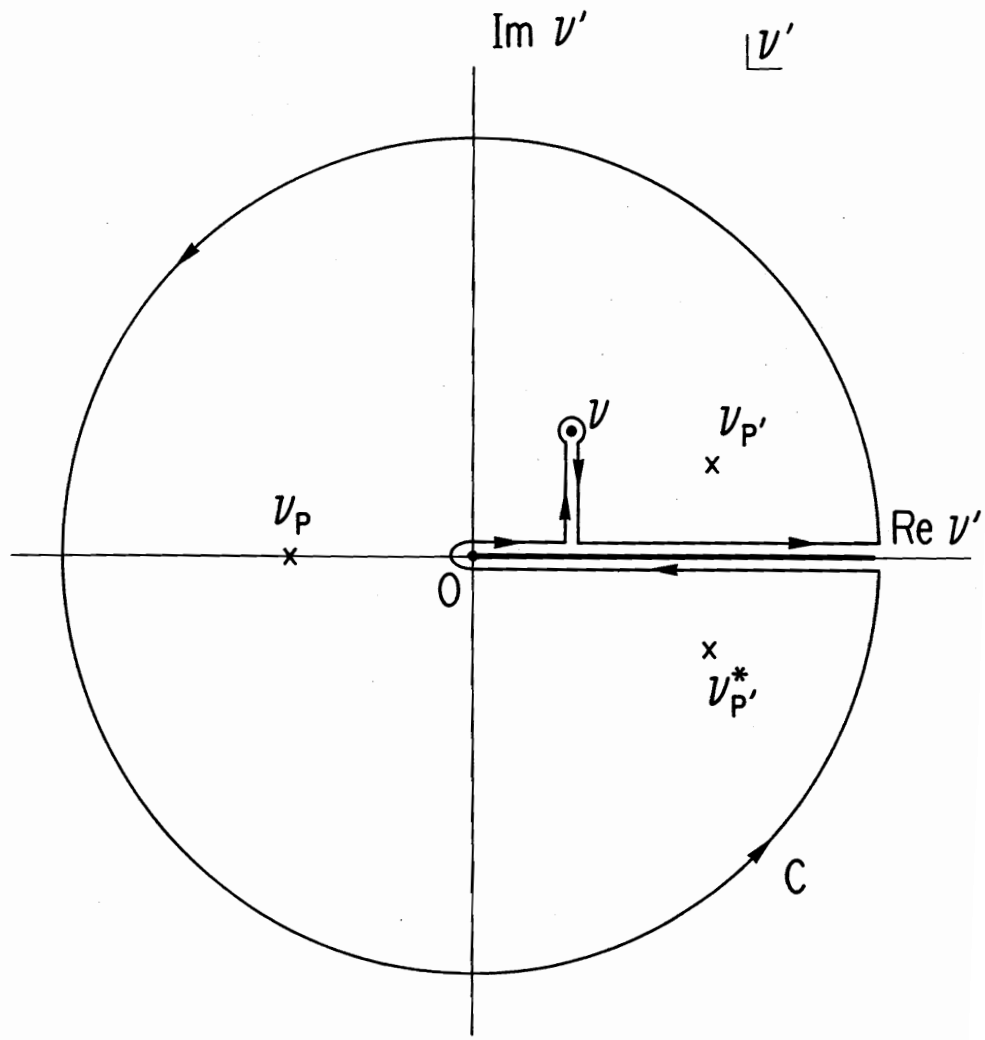

Fig 1

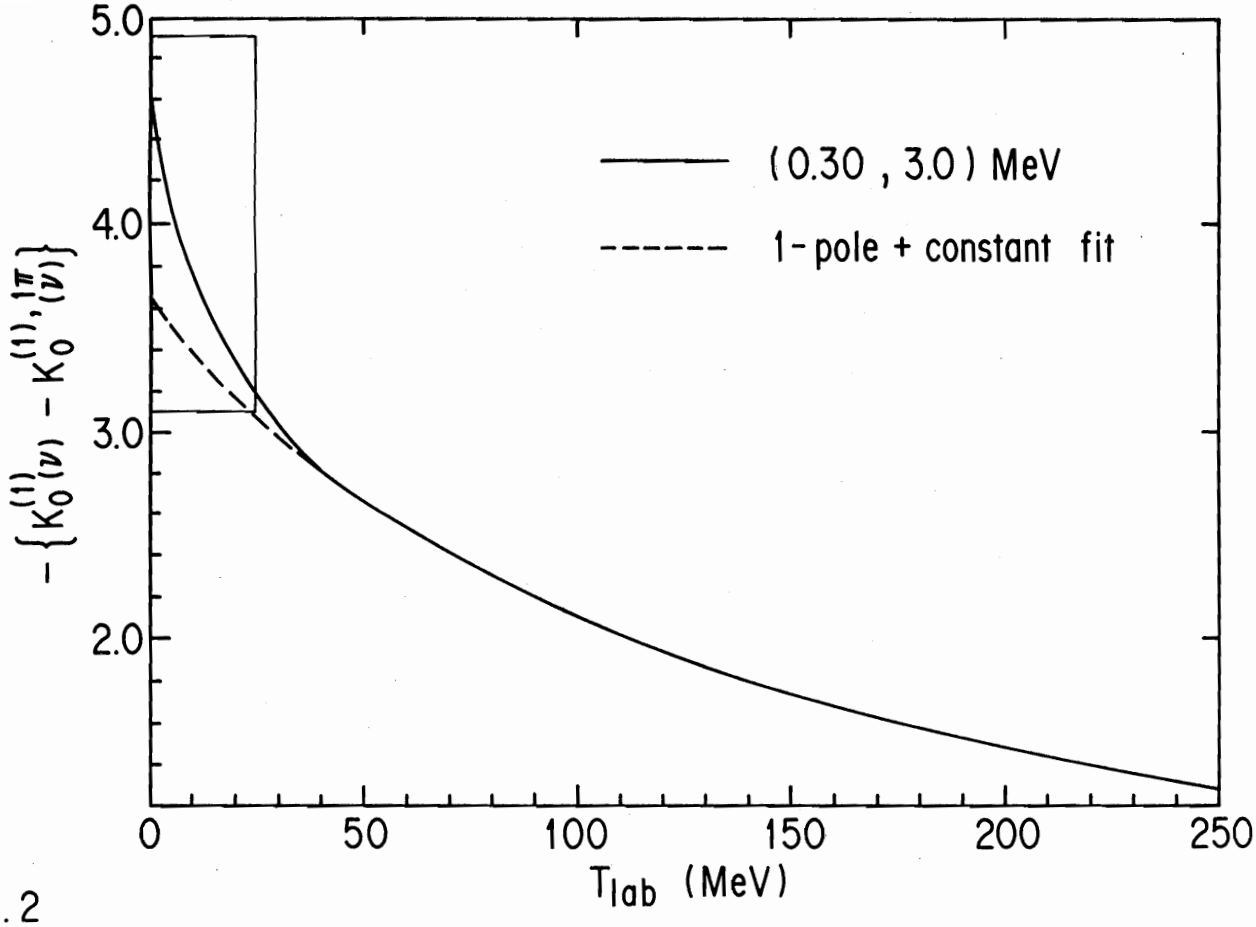
5.0
4.0
3.0
2.0
0
50
100
150
200
250
T_{lab} (MeV)
$-\left\{K_0^{(1)}(\nu) - K_0^{(1),1\pi}(\nu)\right\}$
(0.30 , 3.0) MeV
1-pole + constant fit

Fig. 2

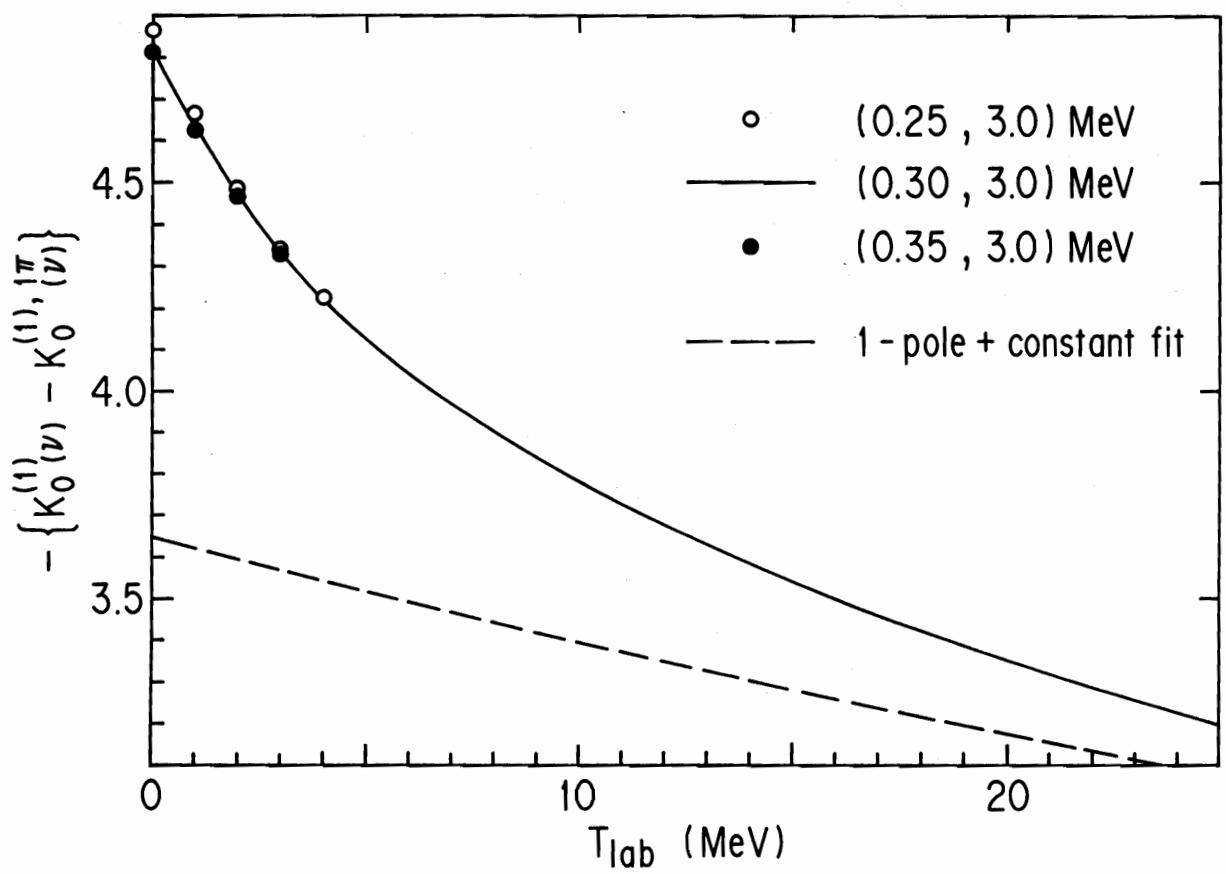
4.5
4.0
3.5
0
10
20
T_{lab} (MeV)
$-\left\{K_0^{(1)}(\nu) - K_0^{(1),1\pi}(\nu)\right\}$
(0.25 , 3.0) MeV
(0.30 , 3.0) MeV
(0.35 , 3.0) MeV
1-pole + constant fit

Fig. 3

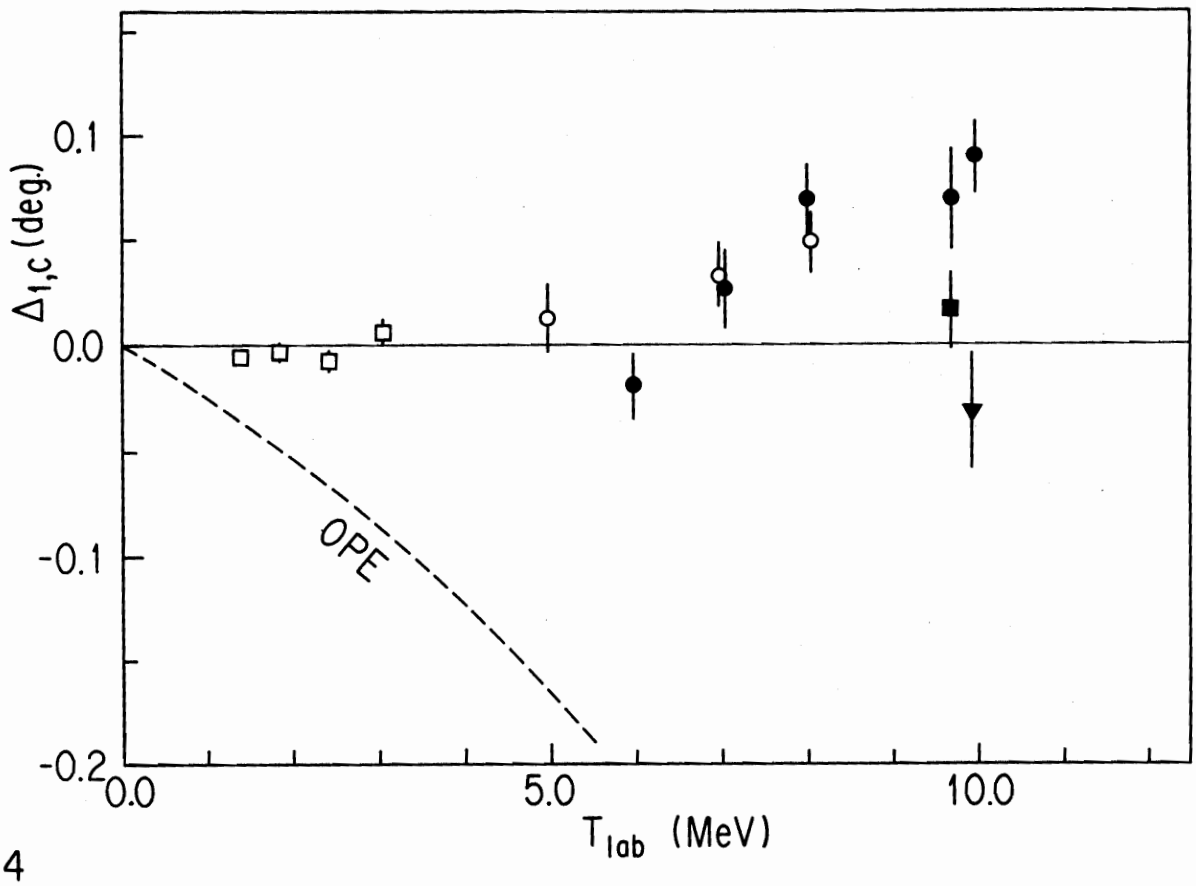
0.1
0.0
-0.1
-0.2
$\Delta_{1,c}$ (deg.)
OPE
0.0
5.0
10.0
T_{lab} (MeV)

Fig. 4

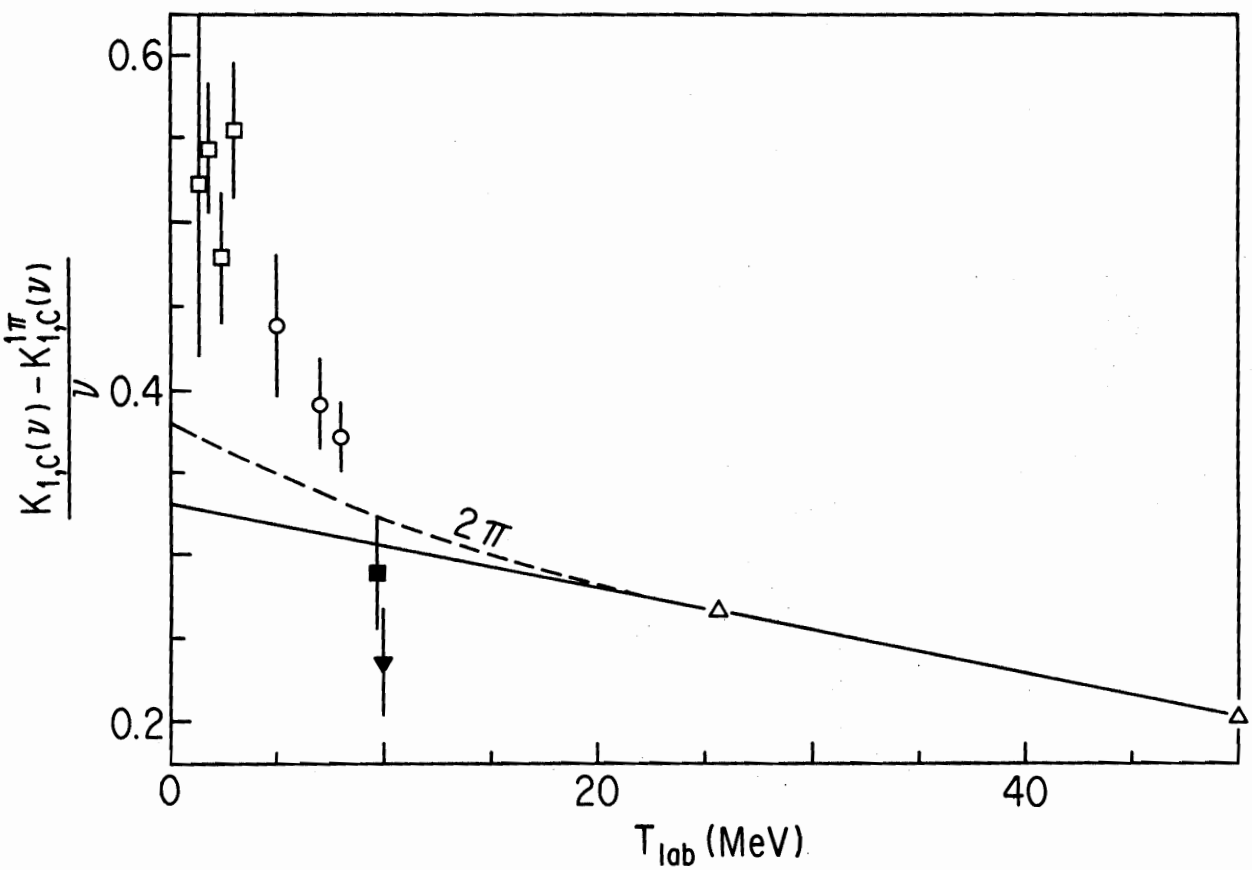
0.6
0.4
0.2
$\frac{K_{1,c}(\nu) - K^{1\pi}_{1,c}(\nu)}{\nu}$
2π
0
20
40
T_{lab} (MeV)

Fig. 5

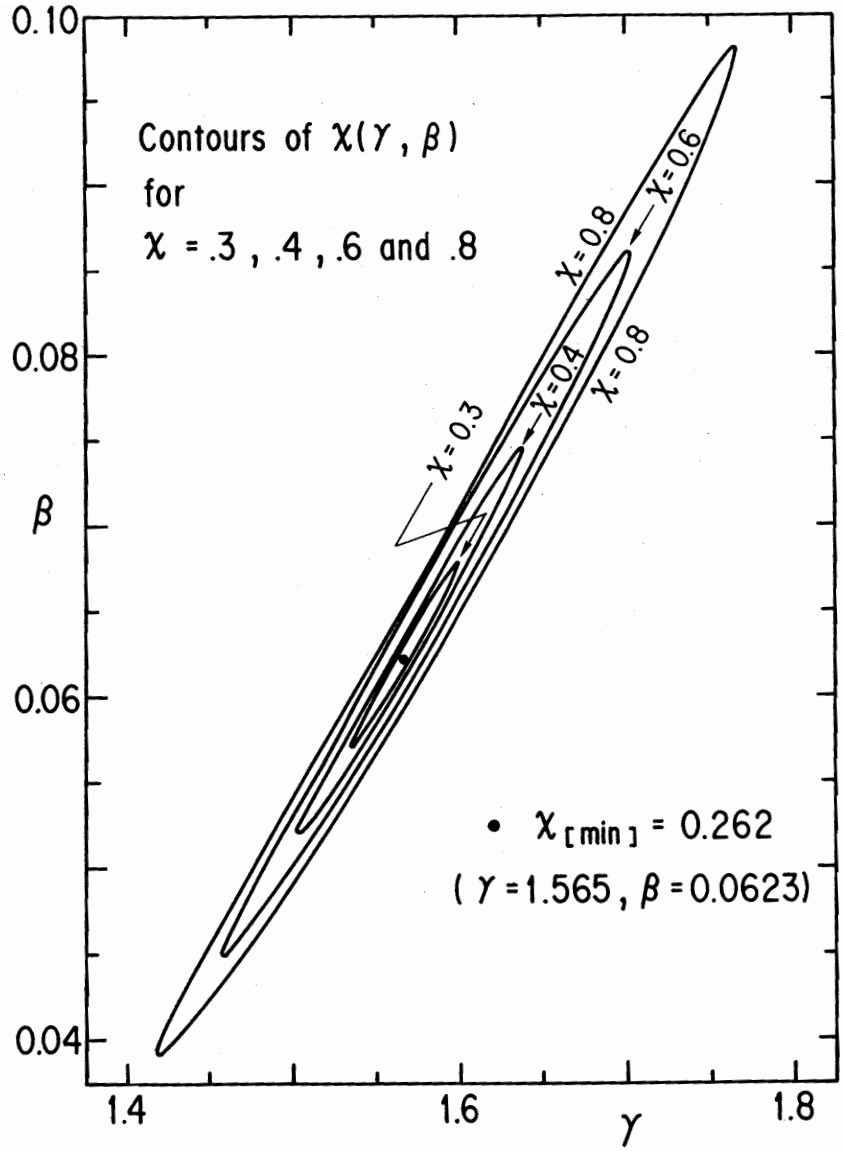
Contours of χ(γ, β)
for
χ = .3 , .4 , .6 and .8
χ=0.6
χ=0.8
χ=0.4
χ=0.8
χ=0.3
• χ[min] = 0.262
(γ=1.565, β=0.0623)
0.10
0.08
0.06
0.04
β
1.4
1.6
1.8
γ

Fig. 6

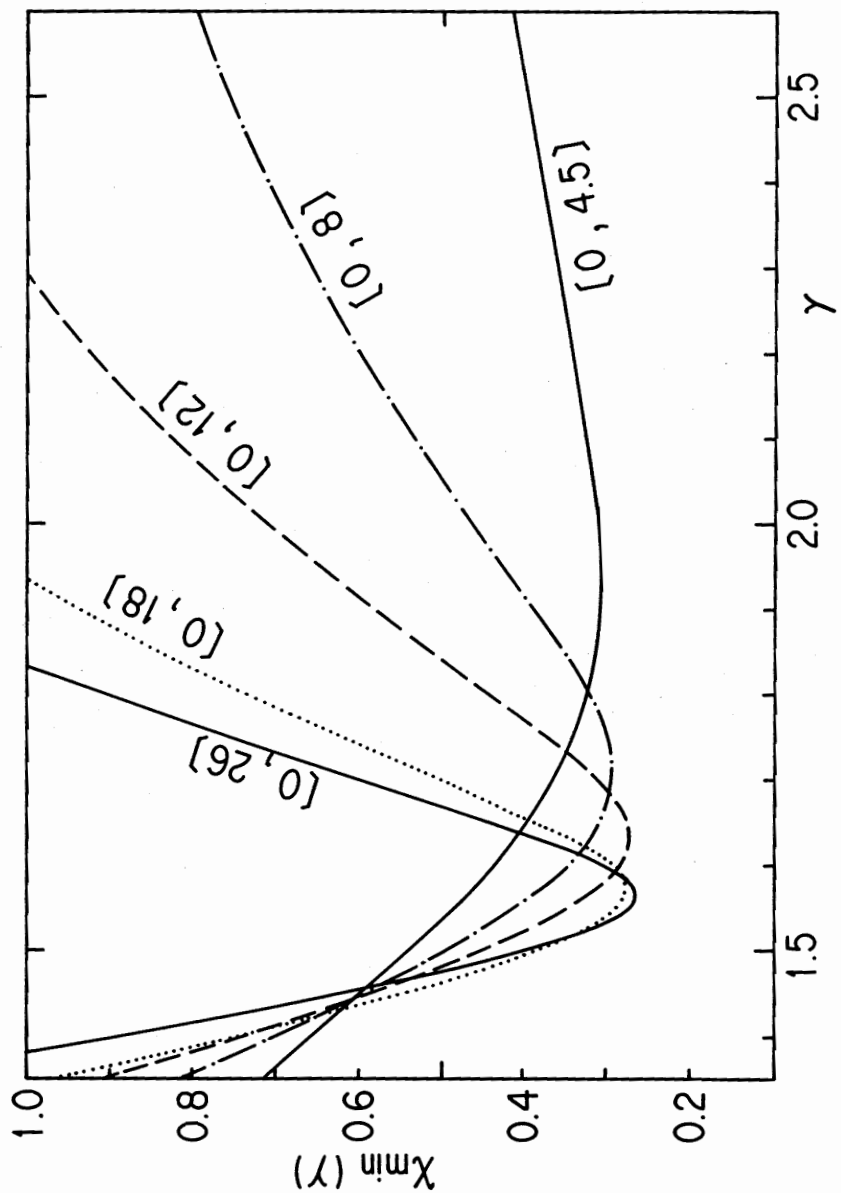
[0, 4.5]
[0, 8]
[0, 12]
[0, 18]
[0, 26]
1.0
0.8
0.6
0.4
0.2
χmin (γ)
1.5
2.0
2.5
γ

Fig. 7

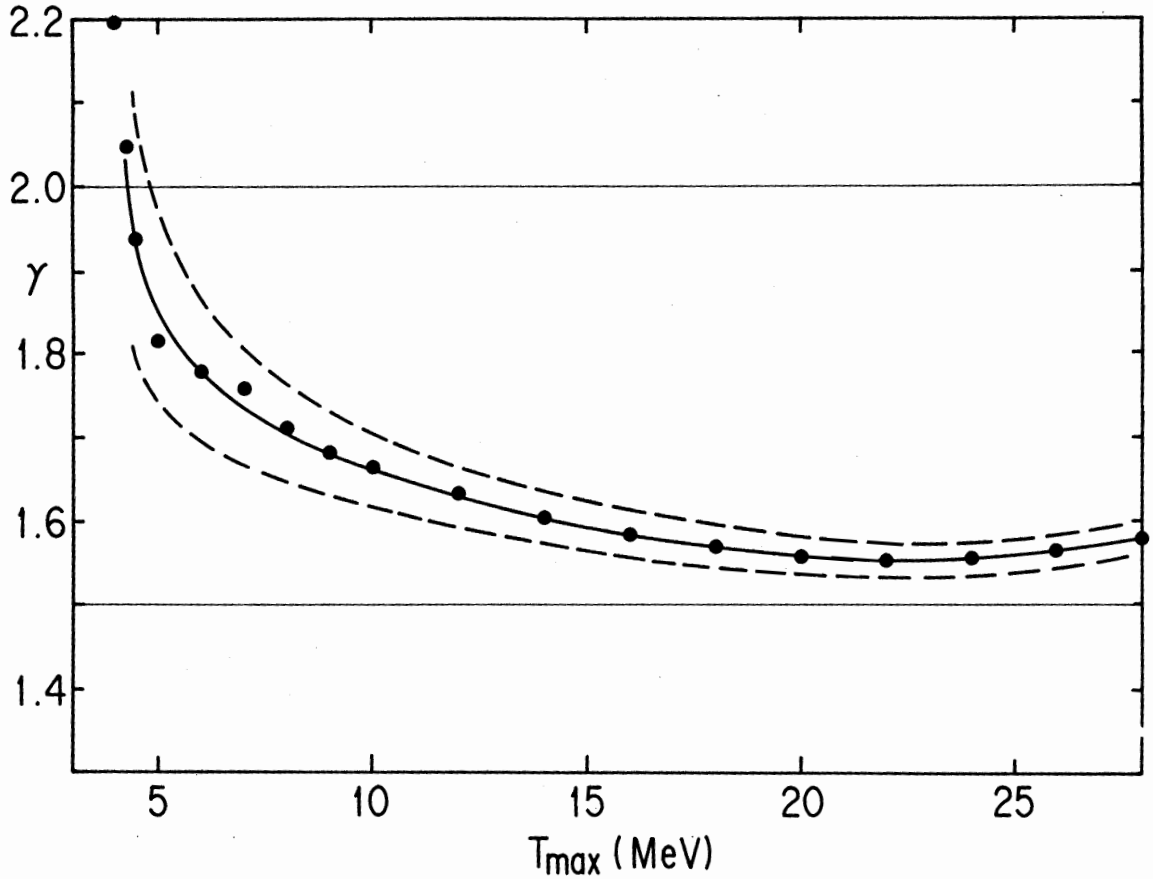

Fig.8

NAME	I.D No	M.S.

RETURN TO FERMILAB LIBRARY